Diffusion in Three-Dimensional Liouvillian Maps

Oreste Piro[a] and Mario Feingold
The James Franck Institute, The University of Chicago, Chicago, Illinois 60637
(Received 6 July 1988)

It is shown that chaotic trajectories in volume-preserving flows, $\dot{\mathbf{r}}=\mathbf{u}_\epsilon(x,y,z,t)$, which are arbitrarily close to integrability, $0<\epsilon\ll 1$, can be either trapped or diffusive throughout the available space. A classification of these flows is proposed which both distinguishes and predicts the appropriate type of behavior. In the unbounded case, a new mechanism of diffusion is found which combines motion on the resonances with an adiabatic drift. This process is reminiscent of Arnol'd diffusion.

PACS numbers: 05.45.+b

Temperature, small particles, the concentration of a second fluid, and the magnetic field in highly conducting media represent only a few examples of quantities which, under certain conditions, are passively driven in fluid flows. The study of their dynamics is relevant to the topics of convection,[1] the interpretation of flow visualization experiments,[2] theory of mixing,[3] and the fast dynamo effect,[4] respectively. All these problems can be jointly studied by employment of the idealized concept of passive scalars.[5] For example, in experimental fluid mechanics, powders of particles are used for flow visualization.[2] These particles are small enough such as not to perturb the velocity field, $\mathbf{u}(x,y,z,t)$, but also big enough in order to avoid diffusion. Under these conditions the equation of motion for one passive scalar

$$\dot{\mathbf{r}}=\mathbf{u} \tag{1}$$

is a highly nontrivial dynamical system, L. We shall study only velocity fields which are periodic in x, y, z, and t and also satisfy incompressibility, $\nabla\cdot\mathbf{u}=0$. The latter implies that Eq. (1) is a volume-preserving (in short Liouvillian) dynamical system. The stroboscopic map of Eq. (1) is defined on the three-torus and is also Liouvillian.

Recently, a great deal of work has been devoted to the investigation of the particular cases of Eq. (1) in which either $\mathbf{u}\equiv\mathbf{u}(x,y,t)$ (Refs. 3,5–7) or $\mathbf{u}\equiv\mathbf{u}(x,y,z)$.[8] In both instances, two-dimensional surfaces invariant under the time evolution of L are found for small but finite departures from integrability governed by the parameter ϵ. As a consequence, chaotic trajectories are trapped and do not visit the entire three-torus. At least for the $\mathbf{u}(x,y,t)$ case this behavior is to be expected since Eq. (1) becomes equivalent to a one-degree-of-freedom Hamiltonian system. The purpose of this Letter is twofold. First, we show that nearly integrable trajectories in the general case are by no means necessarily trapped. In this context, we shall propose a classification of the possible dynamical behaviors of Liouvillian maps (L) for small ϵ into four categories according to the form of the corresponding integrable case ($\mathbf{L}^0$); only the first two of those display trapped motion. Second, we describe a novel type of diffusion found in the last category of Liouvillian maps which is reminiscent of Arnol'd diffusion.[9]

We begin with the classification of the L maps, $\mathbf{L}:T^3\to T^3$.[10,11] Using a natural extension of concepts from Hamiltonian mechanics, we can split the three variables into actions and angles $\mathbf{I}\in T^k$, $\boldsymbol{\theta}\in T^{3-k}$, where $k=0,1,2,3$, such that the integrable cases, $\mathbf{L}_k^0$, are

$$\begin{aligned}\mathbf{I}'&=\mathbf{I}\,,\\ \boldsymbol{\theta}'&=\boldsymbol{\theta}+\boldsymbol{\omega}(\mathbf{I})\,.\end{aligned} \tag{2}$$

Clearly, $\mathbf{L}_k^{(0)}$ are uniform translations on $(3-k)$-tori embedded in T^3. Small perturbations of $\mathbf{L}_k^0$, $\mathbf{L}_k=\mathbf{L}_k^0+\epsilon P(\mathbf{I},\boldsymbol{\theta})$, exhibit widely different behaviors. Since $\mathbf{L}_3^0$ is the identity map, $\mathbf{L}_3$ is a small perturbation around the time-independent particular case, $\mathbf{u}\equiv\mathbf{u}(x,y,z)$. It is therefore expected and found that $\mathbf{L}_3$ displays chaotic trajectories which are bounded between Kol'mogorov-Arnol'd-Moser-type (KAM) invariant surfaces.

Interestingly, the chaotic trajectories of $\mathbf{L}_1$ are also trapped. The invariant objects of the corresponding integrable case, $\mathbf{L}_1^0$, are two-tori which separate T^3 into disconnected regions. For $0<\epsilon\ll 1$, most of the two-tori are preserved in a KAM-type manner. However, if the equation

$$m\omega_1(I^*)+n\omega_2(I^*)=2\pi k \tag{3}$$

is satisfied for $m,n,k=$integers, a thin layer of two-tori around I^* will degenerate in a finite number of fixed lines. By a Poincaré-Birkoff-type mechanism, half of those are stable and half are unstable. While chaotic motion appears around the unstable fixed lines, elliptic tubes surround the stable ones.

On the other hand, the trajectories of $\mathbf{L}_0$ are always chaotic. This behavior is to be expected according to the conservative version of the Ruelle-Takens scenario[12,13] and will not be considered here any further.

We are particularly interested in the dynamics generated by $\mathbf{L}_2$ maps and we shall devote the remainder of this Letter to its understanding. In this case there are nearly integrable trajectories that cover the entire three-

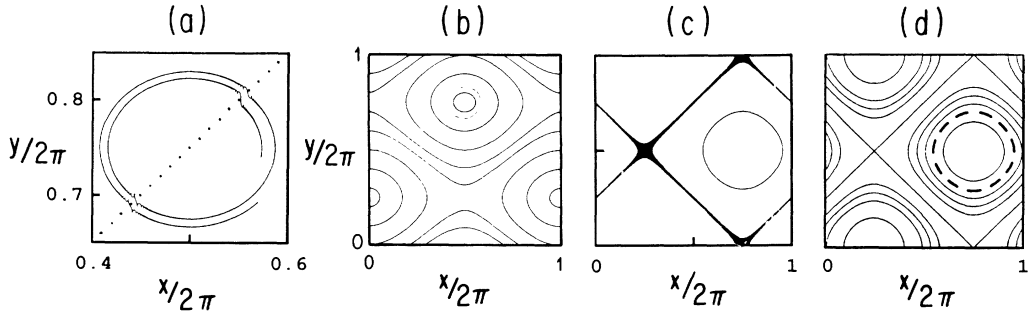

FIG. 1. Trajectories and theoretical predictions for the case $\omega_z(x,y)=C_1\cos y+B_2\sin x$ with $C_1=B_2=4$. Also $\alpha_{A1}=1$, $\alpha_{A2}=2.5$, $\alpha_{B1}=1.5$, and $\alpha_{C2}=2$. In this case $\Gamma_{(1,k)}$ cross all Σ_β at least once and therefore a single trajectory will cover the entire T^3 for arbitrarily small ϵ. (a) Projection on the actions plane of one trajectory at $\epsilon_A=\epsilon_R=10^{-3}$. The dotted line is the $\Gamma_{(1,0)}$ surface. In order to emphasize the resonant jumps, only a small fraction of the plane is shown. (b) Some of the level curves of $H_0(x,y)$ (solid lines) and the first turn of the trajectory shown in (a) (dashed line). (c) Two trajectories at $\epsilon_A=0$ corresponding to the $(n,k)=(1,0)$ and $(125,-23)$ resonances, respectively. (d) The resonant surfaces of Eq. (8) with $n\leq 3$ (solid lines) and the $(n,k)=(125,-23)$ trajectory (dashed line).

torus. In order to illustrate the mechanism of diffusion in $\mathbf{L}_2$ maps, let us consider

$$x'=x+\epsilon_R\alpha_{A1}\sin z+\epsilon_A\alpha_{C2}\cos y\,,$$
$$y'=y+\epsilon_A\alpha_{B1}\sin x'+\epsilon_R\alpha_{A2}\cos z\,, \tag{4}$$
$$z'=z+\omega_z(x',y')\,.$$

This example should be regarded as a truncated Fourier expansion of the most general perturbation around an $\mathbf{L}_2^0$-type integrable case. In Eq. (4), ω_z, α_{A1}, α_{B1}, α_{C2}, and α_{A2} are ~ 1, while ϵ_R and ϵ_A are much smaller. For the first part of the discussion we assume $\epsilon_R=\epsilon_A=\epsilon$. The integrable case, $\mathbf{L}_2^0$, is obtained when $\epsilon=0$. Here, the trajectories lie on lines for which the actions (x,y) are constant. The motion on these lines is parametrized by the value of the angle, z. Extrapolating the conclusions of the KAM theorem, one might expect that under small perturbations ($\epsilon\ll 1$) a finite measure of the invariant lines is only slightly distorted. However, both $O(\epsilon)$ perturbation expansions and numerical experiments disclose a different scenario. All the lines break down and because of an effective drift, coalesce into invariant surfaces roughly parallel to the angle axis, z. This behavior can be understood in terms of an adiabatic approximation. Since the angle (z) changes fast relative to the action variables (x,y), the dynamics of the latter is sensitive only to the averaged z dependence. In the $\epsilon\to 0$ limit and if $\omega_z(x,y)$ is irrational, we can assume that z will cover the entire $(0,2\pi)$ interval before the actions have changed significantly. Since in the case of Eq. (4), $\langle\sin z\rangle_z=\langle\cos z\rangle_z=0$, the adiabatic motion of the actions is described by the following two-dimensional map:

$$x'=x+\epsilon\alpha_{C2}\cos y\,, \tag{5a}$$
$$y'=x+\epsilon\alpha_{B1}\sin x\,. \tag{5b}$$

In turn, Eq. (5) leads to a system of two ordinary differential equations if $t=\epsilon n$

$$dx/dt=\alpha_{C2}\cos y,\quad dy/dt=\alpha_{B1}\sin x\,, \tag{6}$$

which can be exactly integrated. The trajectories of Eq. (6) are level curves of the $H_0(x,y)$ function

$$H_0(x,y)=\alpha_{C2}\sin y+\alpha_{B1}\cos x=\beta \tag{7}$$

and are depicted in Fig. 1(b). Therefore, according to the adiabatic approximation, the trajectories of Eq. (4) lie on surfaces, $\Sigma_\beta\subset T^3$, which satisfy Eq. (7). However, this approximation will fail whenever the resonance condition

$$n\omega_z(x,y)=2\pi k \tag{8}$$

is satisfied. On the surfaces where Eq. (8) holds, $\Gamma_{(n,k)}\subset T^3$ [see Fig. 1(d)], the angle visits only a finite set of points in the $(0,2\pi)$ interval. Therefore, here the z-dependent terms in Eq. (4) are not averaging out any more and jumps between different Σ_β surfaces take place [see Fig. 1(a)]. Since in Fig. 1(a), ϵ is only 10^{-3}, the influence of the resonances with $n>1$ cannot be seen.

In Fig. 2 we show the value of $H_0(x,y)$ along the trajectory of Fig. 1(a). As predicted by the adiabatic approximation, $H_0(x,y)$ is constant [up to $O(\epsilon)$ oscillations] in between the times when it crosses $\Gamma_{(1,0)}$. In layers of width $O(\epsilon^{1/2})$ around $\Gamma_{(1,0)}$, the $O(\epsilon)$ oscillations diverge and later, after the trajectory exits from the resonant layer, fall off to a different value of β,β', such that $\Delta\beta=|\beta'-\beta|=O(\epsilon^{1/2})$. A more precise description of the behavior in Fig. 1(a) can be obtained from a perturbation expansion. If we write the exact invariant of Eq. (4), $H(x,y,z)=\sum\epsilon^i H_i(x,y,z)$, then to $O(\epsilon)$, the invariance condition $H(x',y',z')=H(x,y,z)$ leads to a linear functional equation for H_1. This can be solved by our setting $H_1=\sum h_n(x,y)e^{inz}$. The a_n-Fourier coefficients satisfy

$$h_n(x,y)[e^{in}\omega(x,y)-1]=-\tfrac{1}{2}\delta_{1,n}(i\alpha_{A1}\alpha_{B1}\sin x-\alpha_{A2}\alpha_{C2}\cos y)+\tfrac{1}{2}\delta_{-1,n}(i\alpha_{A1}\alpha_{B1}\sin x-\alpha_{A2}\alpha_{C2}\cos y)\,, \tag{9}$$

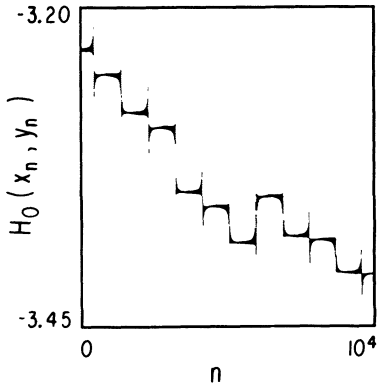

FIG. 2. Adiabatic invariant $H_0(x_n,y_n)$ vs n. The trajectory is the same as in Fig. 1(a), but 2×10^4 instead of 0.7×10^4 iterations are shown.

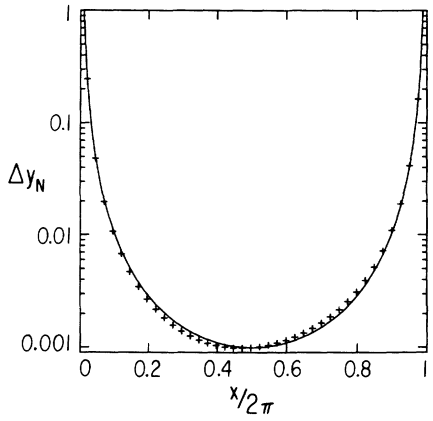

FIG. 3. Theoretical (solid line) and numerical (crosses) displacements in y, $\Delta y_N=(y_N-y_0)/2\pi$ for $\omega_z(x,y)=x$, $\epsilon_A=0$, and $N=2\times10^4$. The adiabatic α parameters are the same as in Fig. 1.

and therefore are singular on the $\Gamma_{(1,k)}$ surfaces. In general, the coefficients of H_i will diverge on the $\Gamma_{(i,k)}$ resonant surfaces of Eq. (8). If in Fig. 2 we replace $H_\epsilon=H_0+\epsilon H_1$ instead of H_0, the $O(\epsilon)$ oscillations are suppressed [become $O(\epsilon^2)$] and consequently jumps are observed when crossing $\Gamma_{(2,k)}$ surfaces as well.

To make further progress in understanding the behavior of $\mathbf{L}_2$ maps, we need to distinguish between ϵ_A and ϵ_R in Eq. (4). When $\epsilon_R=0$, the actions which are now decoupled from the angle change according to Eq. (5). Therefore, the Σ_β surfaces are exactly invariant.[14] On the other hand, if $\epsilon_A=0$, the actions are coupled only through the dynamics of the angle. Remarkably, this leaves us with a three-dimensional nonintegrable map whose trajectories lie on the $\Gamma_{(n,k)}$ resonant surfaces [see Eq. (8), Figs. 1(c) and 1(d)]. In this case, the time scale of the motion on the $\Gamma_{(1,k)}$ surfaces is $O(\epsilon_R)$, while that on the $\Gamma_{(n,k)}$ resonant surfaces with $n>1$ is $O(\epsilon_R^2)$. Since an $O(\epsilon_R^2)$ effective coupling between the actions appears in $\mathbf{L}_2(\epsilon_A=0)$, this behavior is due to a similar mechanism as the adiabatic motion. Specifically, on a $\Gamma_{(n,k)}$ surface, n consecutive values of the angle are equally distanced in the $(0,2\pi)$ interval.[15] Therefore, in the nth iterate of Eq. (4), the $O(\epsilon_R)$ term in the displacement of the actions vanishes and if the $O(\epsilon_R^2)$ contribution is averaged over the angle,[16] then

$$x_n=x_0-\tfrac{1}{4}\epsilon_R^2\alpha_{A1}\alpha_{A2}\frac{\partial\omega_z}{\partial y}\frac{n}{\sin^2(\omega_z/2)}, \tag{10a}$$

$$y_n=y_0-\tfrac{1}{4}\epsilon_R^2\alpha_{A1}\alpha_{A2}\frac{\partial\omega_z}{\partial x}\frac{n}{\sin^2(\omega_z/2)}. \tag{10b}$$

If we set $t=\epsilon_R^2 n$ in Eq. (10), a system of differential equations is obtained in the $\epsilon_R\to0$ limit. Its trajectories are given by $\omega_z(x,y)=\delta$ and are arbitrarily close to the appropriate $\Gamma_{(n,k)}$ surfaces.

In order to illustrate the usefulness of Eq. (10), we study the case $\omega_z(x,y)=x$ and $\epsilon_A=0$. Here, the y action is passively driven by the well-known two-dimensional standard map. In Fig. 3 the numerically obtained displacement in y, Δy, is compared with the theoretical prediction of Eq. (10). Clearly, the divergence of Δy at $x=0$ corresponds to the $O(\epsilon_R)$ motion on the $\Gamma_{(1,0)}$ surface.

In view of these results, it is natural to assume that to first approximation the dynamics of Eq. (3) when both ϵ_A and ϵ_R are finite, $0<\epsilon_A,\ \epsilon_R\ll1$, is a superposition of adiabatic motion on Σ_β and resonant motion on $\Gamma_{(1,k)}$. Let us use this picture to estimate the appropriate diffusion rate. While the number of iterations the trajectory moves adiabatically is $N_A=O(\epsilon_A^{-1})$ (between two consecutive crossings of $\Gamma_{(1,k)}$), inside the first resonance it spends $N_R=O(\epsilon_R^{1/2}\epsilon_A^{-1})$. In the estimation of N_R we have assumed that, while inside the $n=1$ resonance, the trajectory pursues its adiabatic motion at the same

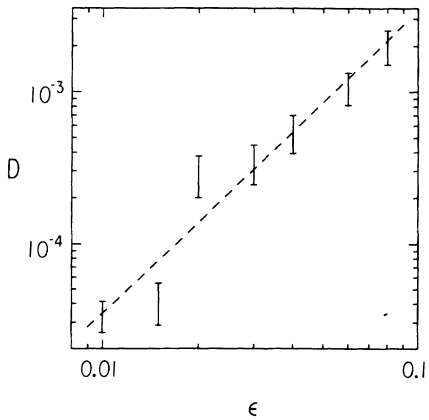

FIG. 4. Diffusion constant vs ϵ. Here $\epsilon_A=\epsilon_R=\epsilon$, $\omega_z(x,y)=x$, and the α's are as in Fig. 1. Error bars are obtained numerically. The best fit (dashed line) for $D\propto\epsilon^a$ gives $a=1.99\pm0.3$.

$O(\epsilon_A^{-1})$ rate and in addition proceeds along the $\Gamma_{(1,k)}$ surface with an $O(\epsilon_R^{-1})$ velocity. Accordingly, the jump size is $O(\epsilon_R^{3/2}\epsilon_A^{-1})$ and if we assume that its direction is random, the diffusion constant $D=O(\epsilon_R^3\epsilon_A^{-1})$ is obtained. Numerically, we find that over time scales much larger than the autocorrelation time, trajectories are indeed diffusive. Moreover, when $O(\epsilon_R)\leq O(\epsilon_A)$ we find good agreement between our estimate for D and numerical experiments (see Fig. 4). However, if $O(\epsilon_R) > O(\epsilon_A)$ trajectories eventually stick to the resonances $\Gamma_{(1,k)}$ and the hypothesis leading to our estimate fails. In this regime, the resonant motion becomes dominant and a different diffusion mechanism which requires further investigation settles in.

We should stress that the diffusion in $\mathbf{L}_2$ maps is much faster than the Arnol'd diffusion which appears in N-degrees-of-freedom Hamiltonian systems for $N\geq 3$. For the latter, the coupling between the actions is given by the Nekhoroshev theorem[17] to be exponentially small and, as a consequence, $D=O[\exp(-\epsilon^{-1/2})]$. Moreover, while in the Hamiltonian case diffusion happens through an interconnected web of resonances, in $\mathbf{L}_2$ maps the resonant surfaces, $\Gamma_{(n,k)}$, do not intersect and the available space is covered as a result of the adiabatic motion. As a consequence, in the $\epsilon\rightarrow 0$ limit the resonances with $n>1$ will have a vanishing contribution to the diffusion rate of $\mathbf{L}_2$. Finally, we also point out that the diffusion in $\mathbf{L}_2$ maps might be experimentally observed for passive scalars in the Rayleigh-Bénard system above the oscillatory instability.[18]

We thank L. P. Kadanoff for many useful discussions. This work has been supported in part by the National Science Foundation under Grant No. DMR85-19460. M.F. acknowledges the support of the Dr. Chaim Weizmann Foundation. O.P. acknowledges support by Consejo Nacional de Investigaciones Científicas y Técnicas of Argentina.

[a]Also Departemento di Física, Universidad Nacional de la Plata, C.C. 67, (1900) La Plata, Argentina.

[1]C. Normand and Y. Pomeau, Rev. Mod. Phys. **49**, 581 (1977).

[2]D. J. Tritton, *Physical Fluid Dynamics* (Van Nostrand, Berlin, 1977).

[3]W. L. Chien, H. Rising, and J. M. Ottino, J. Fluid Mech. **170**, 355 (1986).

[4]S. Childress, J. Math. Phys. **11**, 3063 (1970).

[5]H. Aref, J. Fluid Mech. **143**, 1 (1984).

[6]J. Chaiken, R. Chevray, M. Tabor, and Q. M. Tan, Proc. Roy. Soc. London A **408**, 165 (1986).

[7]T. H. Solomon and J. P. Gollub, in *Proceedings of the Fritz Haber International Symposium,* edited by I. Procaccia (Plenum, New York, 1987).

[8]T. Dombre, U. Frish, J. M. Green, M. Henon, A. Mehr, and A. M. Soward, J. Fluid Mech. **167**, 353 (1986).

[9]A. J. Lichtenberg and M. A. Lieberman, *Regular and Stochastic Motion* (Springer-Verlag, Berlin, 1983).

[10]M. Feingold, L. P. Kadanoff, and O. Piro, J. Stat. Phys. **50**, 529 (1988).

[11]M. Feingold, L. P. Kadanoff, and O. Piro, in *Universalities in Condensed Matter,* edited by R. Julllien, L. Peliti, R. Rammal, and N. Boccara (Springer-Verlag, Berlin, 1988).

[12]D. Ruelle and F. Takens, Commun. Math. Phys. **20**, 167 (1971).

[13]S. Newhouse, D. Ruelle, and F. Takens, Commun. Math. Phys. **64**, 35 (1978).

[14]We disregard the consequences of discretizing Eq. (6), since these are both outside the scope of this paper and also do not significantly alter the properties of $\mathbf{L}_2$ maps.

[15]This is correct only if $O(\epsilon_R)$ deviations are neglected.

[16]In this case, z is a fast variable since it changes $O(\epsilon_R)$.

[17]G. Benettin and G. Gallavoti, J. Stat. Mech. **44**, 293 (1986).

[18]T. H. Solomon and J. P. Gollub, Phys. Fluids **31**, 1372 (1988).